Optical and Quantum Electronics (2023) 55:608
https://doi.org/10.1007/s11082-023-04896-5

Al-doped ZnO based long range optical fibre sensor for efficient low refractive index detection

Hemant Kumar[1] · Raj Kumar[1] · Umang Ramani[1] · Bipin K. Singh[2] · Praveen C. Pandey[1]

Received: 18 August 2022 / Accepted: 26 April 2023 / Published online: 14 May 2023

Abstract
In this article, a simulation of surface plasmon resonance (SPR) based Al-doped ZnO (AZO) coated long-range low refractive index detections in infrared range sensor by the finite element method is presented. Plasmonic material Al-doped ZnO is used for SPR conditions in the desired range. The effects of AZO layer thickness on resonance wavelength, confinement loss, and sensitivity of the proposed sensor are examined for different analyte refractive indices. We have optimized coated AZO layer thickness of 90 nm and width of 124.70 µm in our work. The proposed infrared sensor has achieved refractive index sensitivity 2000–16,000 nm/RIU, and the resolution $5.00 \times 10^{-5} - 6.25 \times 10^{-6}$ RIU for the analyte's refractive index range from 1.23 to 1.37. The proposed sensor may be utilized for detecting low refractive index organic chemicals, biomedical, and liquid foods and may also be used in other sensing applications.

Keywords Optical fiber · SPR sensor · Al-doped ZnO · Low refractive index · Infrared region

1 Introduction

From the last three decades, the surface plasmon resonance (SPR) principle is more prevalent in detection of organic chemicals, bio-chemical, gases and other analyte. SPR based optical fiber devices have simple structure, small size, fast response, very sensitive, free-labelling, long-distance transmission and other unique properies (Homola 2008). Surface Plasmon is a collective oscillation of free electrons charge density which is excited by the incident photons and propagates along the interface between metal and dielectric (Alexandre 2012). The SPR condition occurs, when propagation wave vector of incident photons and free electrons on the metal layer are matched together. In this condition a sharp resonance peak appears at a particular wavelength that wavelength is called resonance wavelength. The surface plasmon wave (SPW) is highly sensitive to the slight change in the refractive index of the sensing analyte (Raether 1988; Saeed et al. 2019). The SPR

✉ Praveen C. Pandey
pcpandey.app@iitbhu.ac.in

[1] Department of Physics, India Institute of Technology (BHU) Varanasi, Varanasi 221005, India

[2] Department of Physics, University of Mumbai, Mumbai 400098, India

phenomena are very attractive for sensing applications because they are extremely sensitive to changes in refractive indices of the external medium. This aspect is used in different fields such as medical diagnostics, biochemistry, biological substance, solution concentration measurement, food safety, and environment monitoring (Lee et al. 1999; Gupta et al. 2009; Li et al. 2016; Xing et al. 2015; Paul et al. 2017; Wang et al. 2018). The SPR-based sensors have also been utilized for glucose detection in urine, formalin detection in food items, cancer cells, and other viruses and disease detection (Karki et al. 2022a, b, c).

Conventional photonic crystal fibres, optical waveguides, and prism-metal coated SPR-based sensors are either too heavy or too complicated to operate in the actual condition (Zhao et al. 2014; Harris and Wilkinson 1995; Kretschmann and Raether 1968; Karki et al. 2022d, 2023). Optical fibre offers sensing devices that show various advantages such as simple and flexible design, small size, proper mode guide mechanism, and extreme sensitivity, etc. Shukla et al. (2015) proposed a metal-ZnO bi-layer SPR based fibre sensor that detects the analyte refractive index range from 1.30 to 1.37. The maximum sensitivity was obtained at 3161 nm/RIU in wavelengths between 400 and 800 nm. Kanmani et al. (2019) designed a bi-layer of silver (Ag), and titanium oxide (TiO_2) coated optical fibre sensor for isopropyl alcohol detection that works within the wavelength range 900–1500 nm. The refractive index of solution varies from 1.33 to 1.3597 with different concentrations (0–60%) of isopropyl alcohol in distilled water. Liu et al. (2013) proposed the experimental SPR-based silver deposited hollow fibre (HF) sensor to detect different volume ratios mixed solutions of kerosene and phonymethylphenyl siloxane liquid. Its liquid mixture solution's refractive index has a range of 1.51–1.58. This HF sensor achieved the highest sensitivity 6607 nm/RIU, and resolution 0.8×10^{-4}–2.5×10^{-4} RIU in wavelengths range 400–800 nm. Karki et al. (2022e) proposed the multi-layers metal and oxides-coated surface plasmon biosensor. This biosensor is reported to have a maximum sensitivity 664.6°/RIU at a refractive index 1.37. Nayak and Jha (2017) reported a D-shape SPR-based silver-graphene coated fibre sensor for analyte refractive indices from 1.33 to 1.37 within wavelengths ranging from 600 to 900 nm. The maximum sensitivity and resolution of the sensor are 6800 nm/RIU and 8.0×10^{-5} RIU, respectively. Thus, most fiber sensors detect only high refractive index analytes within visible-infrared regions. Some substances have low refractive indices, such as fluorine-containing organics, liquid CO_2, medical oxygen (Yang et al. 2019), sevoflurane serving as anaesthetics in the medical field (Chen et al. 2019; Haque et al. 2019a), and other analytes. Therefore, detecting low refractive index analyte by the optical fibre sensor in the infrared region is the need of the day.

Zinc oxide (ZnO) doped with aluminum (Al) reveals the enhancement of magnetic, electric, and optical properties. The Al–O (0.192 nm) covalent bonding length is closer to that of Zn–O (0.197 nm), so Al-doped ZnO (AZO) has high conductive (Mridha and Basak 2007). Sensing devices mainly depend on the plasmonic metals and their layer's thickness. Plasmonic metals Copper (Cu), Silver (Ag), and Gold (Au) are the most commonly used to initiate surface plasmon polaritons (SPPs) for SPR conditions (Albrecht et al. 2018). Compared to these metals, AZO is more available at a lower cost and has controllable conductive and optoelectronic properties. Plasma frequency of AZO observes in the near-infrared region (Rhodes and Franzen 2006). Some authors proposed experimentally and theoretically AZO-coated optical fibre based sensors for different applications such as CO gas sensors (Chang et al. 2002), sodium acetate detection sensor (Chi et al. 2018), formaldehyde detection sensor (Tsai et al. 2014), isopropyl alcohol with glycerin detection sensor (Prieto-Cortés et al. 2019) and relative humidity detection sensors (Harith et al. 2015, 2017).

In this work, we propose SPR based AZO coated D-shape single-mode optical fibre sensor in the IR region. The analysis has done by the finite element method (FEM) using

the COMSOL Multiphysics simulation software. By tuning the thickness and width of the AZO layers, the wavelength sensitivity of the sensor is obtained 2000–16,000 nm/RIU for analyte refractive index ranges 1.23–1.37, and corresponding maximum resolution 6.25×10^{-6} RIU for IR region.

2 Methodology

Figure 1a–c show the cross-section view, side view, and set-up diagram of the D-shaped AZO-coated infrared sensor, respectively. In Fig. 1a, different colors represent the fiber core, fiber cladding, Al-doped ZnO layer, and analyte layer. We have depicted these parts in Fig. 1. Step-index single-mode optical fibre with a diameter of core 8.2 µm and cladding of 125 µm has been used for our simulation work. In Fig. 1b, we have depicted the side view of the proposed sensor and AZO-coated etched section, which interacts with sensing material. In Fig. 1c, we have revealed the set-up diagram of the proposed sensor with different operational parts. The physical significance values of all used parameters in our designed structure are shown in Table 1.

Germanium (Ge) doped silica and fluorine (F) doped silica have been used for fibre core and cladding, respectively. The wavelength-dependent refractive index of the core and cladding have measured by Sellmeier's formula (Tan 1998):

$$n^2(\lambda) = 1 + \frac{p_1\lambda^2}{\lambda^2 - q_1^2} + \frac{p_2\lambda^2}{\lambda^2 - q_2^2} + \frac{p_3\lambda^2}{\lambda^2 - q_3^2} \tag{1}$$

where p_1, p_2, p_3, q_1, q_2, q_3 are Sellmeier's coefficients and λ (in µm) is the light source wavelength. Coefficients values of 4% Ge doped silica are $p_1 = 0.6867$, $p_2 = 0.4348$, $p_3 = 0.8966$,

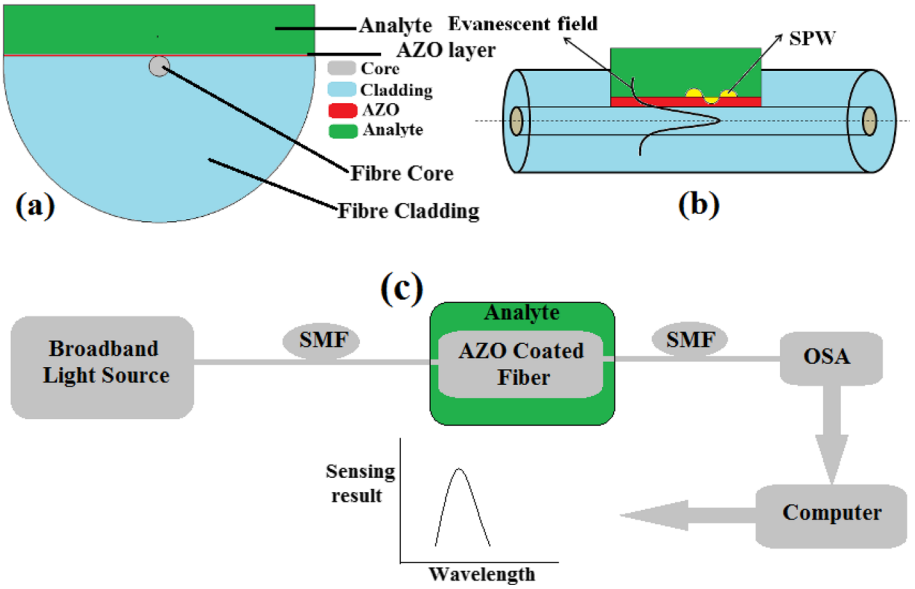

Fig. 1 Schematic diagram of D-shape AZO coated SPR based optical fiber sensor **a** Cross-section view. **b** Side view. **c** Set-up diagram

Table 1 Used parameters values in the proposed fibre sensor model

Parameter	SI unit
Fibre core diameter	8.2 μm
Fibre cladding diameter	125 μm
Optimized AZO layer thickness (t)	90 nm
Optimized AZO layer width (w)	124.57 μm
Taking analyte thickness	20 μm

$q_1 = 0.07268$ μm, $q_2 = 0.1151$ μm, and $q_3 = 10.00$ μm and 1% F doped silica coefficients are $p_1 = 0.696166$, $p_2 = 0.407942$, $p_3 = 0.897479$, $q_1 = 0.068404$ μm, $q_2 = 0.116241$ μm, and $q_3 = 9.89616$ μm (Wang et al. 2019). Using Eq. (1), we have plotted the dispersion spectra for the fibre core and cladding in Fig. 2a.

We have deposited the AZO layer on the etched flat D-shaped optical fibre surface. The AZO layer is used as a plasmonic material to generate the SPR condition. We have analyzed the sensor results for 30–90 nm thick AZO layers with a 20 nm step increment. For AZO, dispersion spectra are defined by the following Drude model (Paliwal and John 2017);

$$\epsilon = \epsilon_\infty - \frac{\omega_p^2}{\left(\omega^2 + \gamma^2\right)} + \frac{i\gamma\omega_p^2}{\omega\left(\omega^2 + \gamma^2\right)} \tag{2}$$

where $\epsilon_\infty (= 3.5)$ represents the background permittivity, γ $(= 4.86 \times 10^{13}$ Hz) is the damping frequency, and ω_p $(= 5.22 \times 10^{14}$ Hz) is the plasma frequency. Here, angular freauency $\omega = \frac{c}{\lambda}$, where c and λ are the speed of light and wavelength, respectively. Figure 2b indicates the AZO metal oxide dispersion curve obtained using the Drude model Eq. (2).

We have used the analytes in the external medium to analyze the sensor's performance, which is direct contact with the AZO layer. Here, we have considered a 20 μm thick analyte medium layer on the AZO layer in our simulation. We have analyzed all the results for the analyte's refractive index range of 1.23–1.37. The dielectric constant (ε_{am}) and refractive index $\left(n_{am}\right)$ of the analyte have the relation $\varepsilon_{am} = n_{am}^2$. The excited surface plasmon resonance (SPR) condition is explained by the Eq. (3) (Shukla et al. 2015).

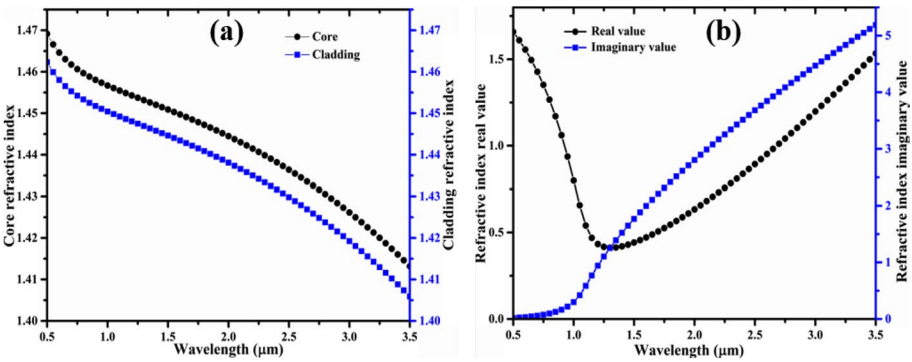

Fig. 2 Dispersion curves for **a** fiber core and cladding, and **b** Al-doped ZnO

$$\frac{2\pi}{\lambda} n_0 sin\alpha = Re(K_{spw}) \tag{3}$$

where $K_{spw} = \frac{\omega}{c}\sqrt{\frac{\varepsilon_{AZO}\varepsilon_{am}}{\varepsilon_{AZO}+\varepsilon_{am}}} = \frac{2\pi}{\lambda}\sqrt{\frac{\varepsilon_{AZO}n_{am}^2}{\varepsilon_{AZO}+n_{am}^2}}$ represents the propagation constant of the SPW and n_0 and c denote the fibre core refractive index and light velocity, respectively. In Eq. (3) left side represents the propagation constant of the incident light source at wavelength λ with an angle α, and right-hand side describes the propagation constant real value of the SPW. In the right side Eq. (3), the propagation constant is changed due to changing the analyte refractive index. Therefore every refractive index satisfied the resonance condition at a particular wavelength. The resonance wavelength shifting can be obtained with the change in the analyte refractive index. The simulation has performed by the finite element method (FEM) using the COMSOL Multiphysics simulation software.

3 Result and discussion

In this paper, the fibre sensor modes characteristics have been analyzed by the finite element method (FEM) using COMSOL multiphysics simulation software. Figure 3a, b illustrate the energy distribution of the core-guided and SPP modes, respectively, for analyte refractive index 1.23. Overall optical energy is enclosed in the fibre core for the core mode condition. The energy distribution presents on the AZO layer and in the analyte medium for the SPP mode condition. The coupled mode phase-matching condition is satisfied when the core and SPP modes are drastically coupled, and more energy is transferred from the core mode to the analyte medium. This energy distribution for the SPR condition is shown in Fig. 3c.

The confinement loss or propagation loss is obtained by the following equation (Haque et al. 2019b):

$$Loss = \frac{54.5757 \times Im(n_{eff}) \times 10^4}{\lambda} \mathrm{dB/cm} \tag{4}$$

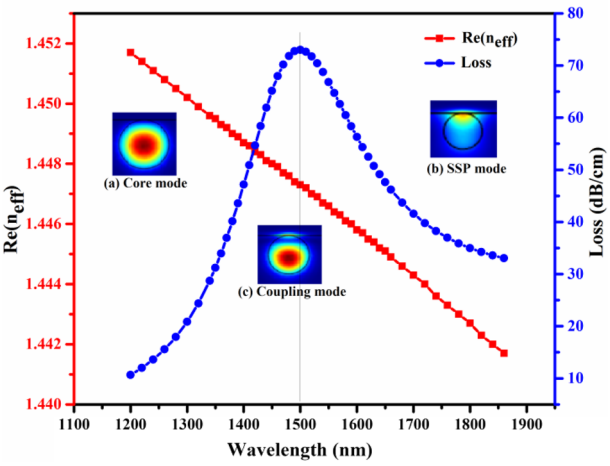

Fig. 3 Variation of real part refractive index and confinement loss spectra of coupling mode with wavelengths at analyte refractive index (n_{am})=1.23, the thickness of AZO layer (t)=90 nm and width (w)=124.57 µm, and the phase matching wavelength represented by the dotted line

where λ (μm) is the source wavelength and $Im(n_{eff})$ indicates the effective coupling mode refractive index imaginary part.

The coupling mode refractive index imaginary part $Im(n_{eff})$ is related to the loss, whereas the real part $Re(n_{eff})$ shows the refractive index in the usual sense. In Fig. 3, the red curve shows the refractive index real part of the effective coupling mode continuously decreasing with the wavelengths. The blue curve represents the confinement loss spectra variation with wavelengths. This loss is determined by the imaginary part of the coupling mode effective refractive index using Eq. (4). The loss spectrum appears upward with a higher value initially. It decreases with a lower value after achieving the maximum loss peak at a resonant wavelength (1500 nm) for the phase-matching coupling condition.

The characteristics of the sensor are determined by the many different performance parameters, i.e., confinement loss, resonant wavelength, sensitivity, and resolution. The AZO plasmonic material generates the surface plasmon wave, and the thickness of the AZO layers affects the SPR phenomenon. Figure 4a exhibits confinement loss spectra curves for 30–90 nm thick AZO layers within the wavelength range from 1060 to 2660 nm for analyte refractive index 1.36. As shown in Fig. 4, the resonance loss peak increases with the thickness of the AZO layer in the red-shift wavelength region.

Figure 4b shows that if the analyte refractive index varies from 1.36 to 1.37, we obtain resonant wavelength shift values of 95 nm and 160 nm for the AZO layer's 70 nm and 90 nm thickness, respectively. Figure 5 illustrates the confinement loss value spectra of the sensor for various widths (40 μm, 60 μm, 80 μm, 100 μm, and 124.70 μm) of the AZO layer for analyte refractive index 1.35 and 1.36. For analyte refractive index 1.35, we have obtained peak loss values 337.8482 nm/RIU, 337.7934 nm/RIU, 337.7386 nm/RIU, 337.7934 nm/RIU, and 337.7600 nm/RIU for 40 μm, 60 μm, 80 μm, 100 μm, and 124.70 μm width AZO layers at constant 1990 nm resonant wavelength, respectively. Also, we have calculated peak loss values 501.4944 nm/RIU, 501.2850 nm/RIU, 501.0494 nm/RIU, 501.2588 nm/RIU, and 501.2588 nm/RIU for different width AZO layers 40 μm, 60 μm, 80 μm, 100 μm, and 124.70 μm, respectively for another refractive index 1.36 at 2085 nm resonant wavelength. According to these data, the resonant wavelength value is fixed, and the peak loss value only minor changes with the width of AZO layers. The confinement loss value represents how much core mode energy is transferred

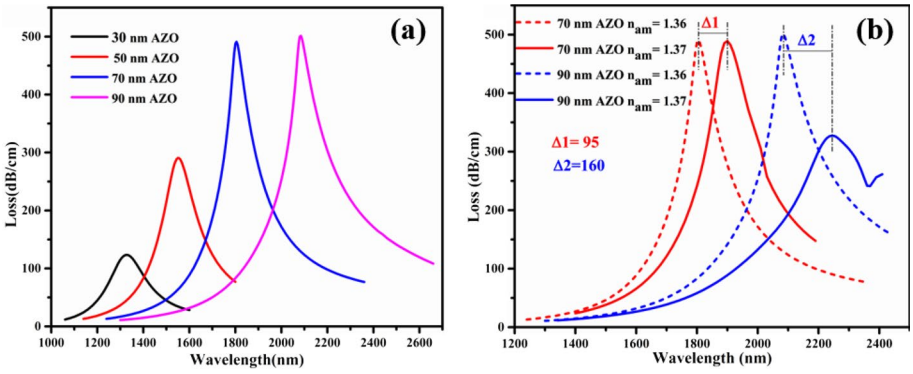

Fig. 4 **a** Change in loss spectra with wavelength for different thicknesses of AZO layers at analyte refractive index 1.36. **b** Loss spectra variation of the sensor for 70 nm and 90 nm thick AZO layers at analyte refractive index 1.36 and 1.37

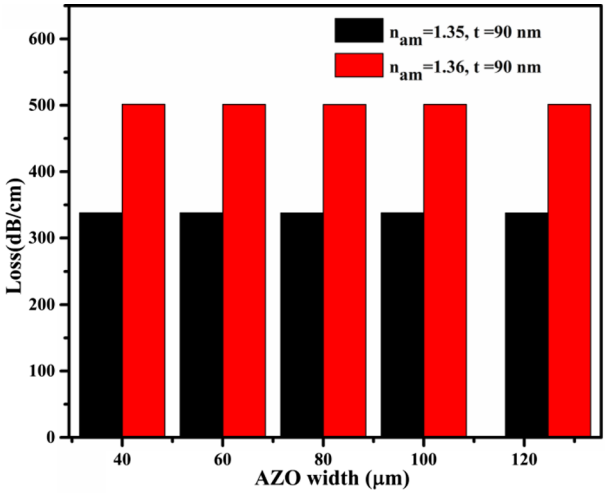

Fig. 5 Variation in losses with widths of AZO layers at a fixed thickness (t) = 90 nm and analyte refractive indices n_{am} = 1.35 and n_{am} = 1.36

to the SPP mode when the external medium analyte is in contact with the AZO layer. We can calculate the change in the external medium analyte's refractive indices by measuring the loss peak shifting values. The wavelength sensitivity of an SPR sensor is defined as the change in the resonant wavelength values per unit change in the refractive index of the external medium, so maximum sensitivity means maximum shifting in resonant wavelength value with a change in two successive refractive indices. If the sensor is highly sensitive, we can be easily calculated the variation in the external medium analyte's refractive indices. The resolution parameter of the SPR sensor expresses the sensor's capability to measure the smallest variation in the analyte's refractive indices.

This D-shape SPR infrared sensor is more sensitive to the external medium refractive index. Figure 6 describes the loss spectra variation of the infrared sensor for analyte refractive indices from 1.23 to 1.37 in the wavelength range 1200–2600 nm. The loss peak value increase with the analyte refractive indices due to strong coupling. We have obtained loss peaks at a resonant wavelength for different analyte refractive indices.

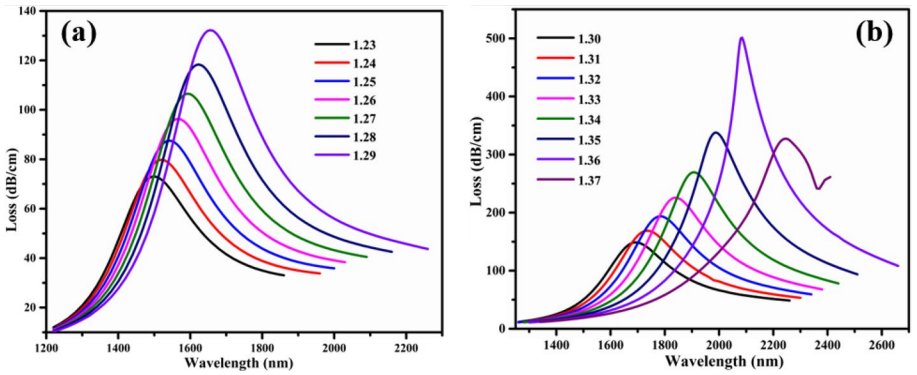

Fig. 6 Variation in loss spectra with wavelengths for different analyte refractive index **a** 1.23–1.29, **b** 1.30–1.37 at fixed thickness (t) = 90 nm and width (w) = 124.70 μm

Figure 7a shows the variation in resonance wavelength with the analyte refractive index for different thick AZO layers. We can see in the figure that the resonance wavelengths of the sensor move to a larger wavelength side, with increases the refractive index of the analyte for all thicknesses of the AZO layers. We have found higher value resonance wavelength for higher value analyte refractive index and lower value resonance wavelength for small value refractive index. It can be clarified by Eq. (3) that the real value of the propagation constant (K_{spw}) of SPW will be higher for a higher value of the analyte refractive index. Hence its SPR condition is obtained at a larger wavelength. Similarly, the SPR condition is obtained at the lower wavelength for the lower value of the analyte refractive index due to the smaller real value of K_{spw} (Sharma and Gupta 2007).

The sensitivity is a significant parameter to examine the performance of the SPR-based fibre sensor. The wavelength interrogation method is mostly used for long wavelength ranges and larger sensitivity SPR sensors. The wavelength sensitivity can be defined as follows in Eq. (5) (Hassani and Skorobogatiy 2009):

$$S_\lambda = \frac{\Delta\lambda_{peak}}{\Delta n_{am}}(\text{nm/RIU}) \tag{5}$$

where $\Delta\lambda_{peak}$ represents the resonant wavelengths shift of two-loss peaks and Δn_{am} indicates the change in two analyte refractive index media.

Figure 7b illustrates the sensitivity variations with the analyte refractive indices for 30 nm, 50 nm, 70 nm, and 90 nm thick AZO layers. It exploits from this figure that the proposed sensor's sensitivity enhances with the AZO layers' thickness. We have optimized a 90 nm thick AZO layer for our sensor for better performance. We have achieved a maximum resolution of 6.25×10^{-6} RIU of the SPR sensor for analyte refractive indices 1.36–1.37, obtained by the following equation (Paul et al. 2019).

$$R = \frac{\Delta\lambda_{min}}{S_\lambda}(\text{RIU}) \tag{6}$$

where $\Delta\lambda_{min}$ (=0.1 nm) is the minimum wavelength instrumental resolution.

We have optimized a 90 nm thick and 124.72 µm width AZO layer for our sensor. Table 2 shows all performance properties of the proposed sensor, i.e., loss peak, resonance wavelength, peak shifting, sensitivity, and resolution. The loss peak values and resonance

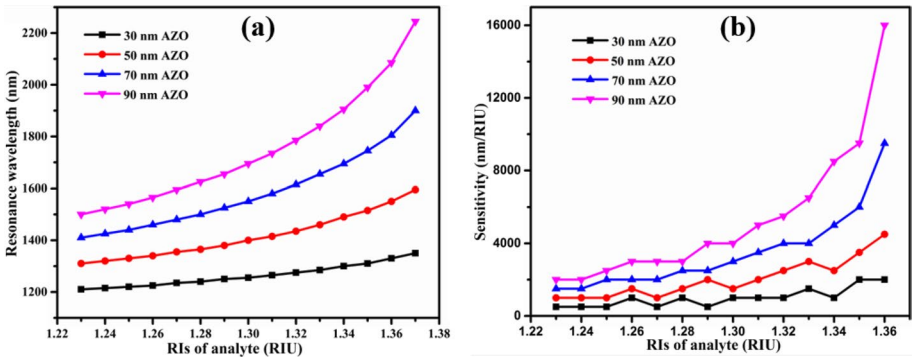

Fig. 7 Variations of the resonance wavelength and sensitivity with analyte refractive indices (RIs) for different thicknesses of AZO layers

Table 2 Performance properties of SPR based D-shaped fiber sensor

Analyte refractive index	Loss peak (dB/cm)	Resonance wavelength (nm)	Peak shifting (nm)	Sensitivity (nm/RIU)	Resolution (RIU)
1.23	73.01	1500	20	2000	5.00×10^{-5}
1.24	79.81	1520	20	2000	5.00×10^{-5}
1.25	87.51	1540	25	2500	4.00×10^{-5}
1.26	96.34	1565	30	3000	3.33×10^{-5}
1.27	106.51	1595	30	3000	3.33×10^{-5}
1.28	118.32	1625	30	3000	3.33×10^{-5}
1.29	132.22	1655	40	4000	2.50×10^{-5}
1.30	148.74	1695	40	4000	2.50×10^{-5}
1.31	168.80	1735	50	5000	2.00×10^{-5}
1.32	193.65	1785	55	5500	1.81×10^{-5}
1.33	225.68	1840	65	6500	1.54×10^{-5}
1.34	269.46	1905	85	8500	1.18×10^{-5}
1.35	337.77	1990	95	9500	1.05×10^{-5}
1.36	501.26	2085	160	16,000	6.25×10^{-6}
1.37	327.31	2245	NA	NA	NA

wavelengths of the sensor vary from 73.01 to 327.31 dB/cm and 1500–2245 nm, respectively. Besides, the wavelength sensitivity of the sensor varies from 2000 nm/RIU to 16,000 nm/RIU for analyte refractive index range 1.23–1.37. This refractive index range covers the many organic chemicals, bio-chemical, different chemical mixtures, and liquid food such as fluorine-containing organics with various concentrations, i.e. 1,1,1-trifluoroacetone ($n_{\mathrm{am}}<1.30$), 1,1,1,3,3,3-hexafluoro-2-propanol ($n_{am}=1.275$), 2,2,2-trifluoroethyl triflu-oroacetate ($n_{am}=1.2812$), trifluoroacetic acid ($n_{am}=1.2850$), 2,2,2-trifluoroethanol ($n_{\mathrm{am}}=1.2907$), heptafluorobutyric acid ($n_{am}<1.30$), trifluoroacetic anhydride ($n_{am}<1.30$) (Dean 1998), savoflurane ($\mathrm{n_{am}}=1.27$) used in medical field for anesthetic (Chen et al. 2019), pure honey ($\mathrm{n_{am}}=1.356$) (Yadav et al. 2020) and other low refractive indices analyte. Table 3 shows the comparison of our work with other authors' previously reported work.

Compared to other optical fibre, prism, grating coupling, and photonic crystal fibre (PCF) based SPR sensors, the proposed sensor has many advantages such as a simple structure, easy and cheap manufacturing, lightweight device, cheap consisting material AZO compared to costly material Gold, Platinum, etc., and detection of the low refractive index analytes. Using AZO layer in our sensor has more advantages such as significant mechanical strength, not easily oxidized with the contact of the external medium, chemical and thermal stability, high optical gain, and excitation binding energy and making it an ideal material to realize excitonic devices at room temperature (Ma et al. 2004). The sensing medium in the proposed sensor structure easily contacts the AZO layer, making it very easy to detect their sensing variations. The sensing medium does not require filling in the hollow core or inside the hole of fibre like other sensors.

We have theoretically demonstrated the performance of our proposed sensor by using the finite element method (FEM) based COMSOL multiphysics simulation software. Better performance results are only meaningful if the designed structure can be experimentally fabricated. Our sensor structure design is very simple, so it can be

Table 3 Performance comparison of low refractive index detection SPR sensor

References	Type of sensor	Max. sensitivity (nm/RIU)	Resolution (RIU)	RI range
Liu et al. (2018)	PCF sensor	6000	2.80×10^{-5}	1.27–1.36
Yang et al. (2019)	PCF sensor	10,700	9.93×10^{-6}	1.19–1.29
Liu et al. (2020)	PCF sensor	15,000	6.67×10^{-6}	1.22–1.33
Wang et al. (2018)	PCF sensor	13,500	7.41×10^{-6}	1.27–1.32
Chen et al. (2019)	PCF sensor	11,055	9.05×10^{-6}	1.20–1.29
Jain et al. (2022)	PCF sensor	10,000	2.00×10^{-5}	1.35–1.40
Singh et al. (2020)	Optical fibre sensor	3725	2.68×10^{-5}	1.27–1.33
Mishra and Mishra (2021)	Optical fibre sensor	10,280	9.72×10^{-6}	1.33–1.38
Kaur et al. (2022)	Optical fibre sensor	10,766.28	9.29×10^{-6}	1.33–1.37
Bag et al. (2020)	Experimental optical fibre sensor	70	5.90×10^{-5}	1.333–1.345
Zhang et al. (2020)	Experimental optical fibre sensor	3973.8	1.51×10^{-5}	1.3415–1.401
Our work	Optical fibre sensor	16,000	6.25×10^{-6}	1.23–1.37

easily fabricated by using laser micro-machine and side-polishing techniques. These techniques are very simple and most convenient for controlling the depth of the fibre and fabrication of D-shaped fibre. After constructing the D-shaped optical fibre, it must be coated with the Al-doped ZnO plasmonic material for SPR condition. The optical fibre can be deposited using many authentic techniques such as high-pressure micro-fluidic chemical deposition, chemical vapor deposition, electron beam evaporation, atomic layer deposition, wheel polishing, and liquid phase deposition (Islam et al. 2020, 2022; Sazio et al. 2006; Shi et al. 2006; Kumar et al. 2021). The thin Al-doped ZnO layer deposition is very easy to achieve using different conventional deposition techniques. Harith et al. (2017) proposed a humidity sensor with Al-doped ZnO layer, which was developed using the well-known and simplest sol–gel method. Although different methods can construct the proposed sensor structure, a question remains whether optical fibre sensor structure parameter dimensions can be exactly maintained in the experimental study. In the actual scenario, when fabricating the device, we generally face ± 1–5% changes in the optimized parameters (Al Mahfuz et al. 2020). In Fig. 5, the loss values are almost the same, and the resonant wavelength has also remained the same with AZO layer width (w) variations. Therefore the sensor performance is unaffected by the deviation of the AZO layer width. For ± 5% deviation of the thickness (t) from their optimized value, we have calculated the alteration of the sensor performance and demonstrated the effect of AZO layer thickness (t) on the loss in Fig. 8. We find the 8 nm shift in resonant wavelength toward the lower wavelength side for − 5% deviation and the 7 nm shift toward the lower wavelength side for + 5% deviation in AZO layer thickness. These small variations in resonant wavelength will have negligible effects on the sensor results. Our structure can tolerate the ± 5% range fabrication error without any change in sensor performances.

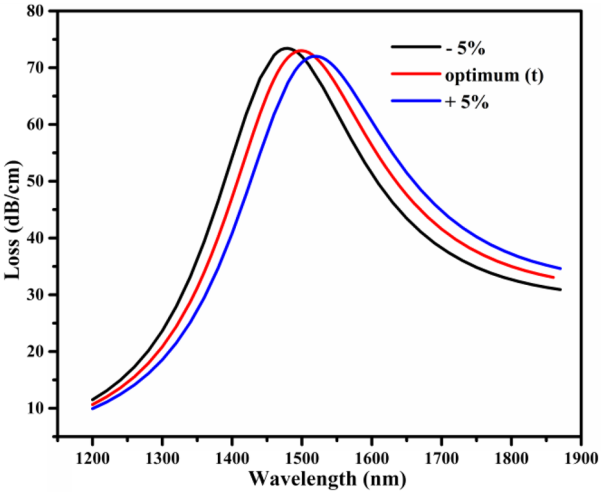

Fig. 8 Loss curve at refractive index 1.23 with ± 5% variation in AZO layer thickness (t)

4 Conclusion

The SPR-based novel D-shape sensor is designed, and it is a numerical analysis by the finite element method (FEM) for low refractive index analyte detection has been made. For SPR conditions, Al-doped ZnO (AZO) has been used as plasmonic material. Our structure is easy to design as only a single layer of AZO is coated on polished D-shape fiber. The proposed SPR sensor has achieved the wavelength sensitivity 2000–16,000 nm/RIU for analyte refractive indices range 1.23–1.37 by adjusting the thickness of the AZO layer. The maximum resolution is obtained at 6.25×10^{-6} for analyte refractive indices range 1.36–1.37. The SPR sensor has a high potential to detect low refractive index analytes, i.e., drug inspection and monitoring, biological and organic species, and other analytes.

Acknowledgements Bipin K. Singh is thankful to the University Grants Commission (UGC), India, for providing financial support through a Dr. D. S. Kothari Postdoctoral Fellowship.

Author contributions All the authors have significant contribution in this paper.

Funding The authors received no specific funding for this work.

Data availability Data and code of this work will available from the corresponding author upon reasonable request.

Declarations

Conflict of interest The authors declare that they have no conflict of interest.

References

Al Mahfuz, M., Hossain, M.A., Haque, E., Hai, N.H., Namihira, Y., Ahmed, F.: Dual-core photonic crystal fiber-based plasmonic RI sensor in the visible to near-IR operating band. IEEE Sens. J. **20**(14), 7692–7700 (2020)

Albrecht, G., Ubl, M., Kaiser, S., Giessen, H., Hentschel, M.: Comprehensive study of plasmonic materials in the visible and near-infrared: linear, refractory, and non-linear optical properties. ACS Photonics **5**(3), 1058–1067 (2018)

Alexandre, G.B.: Plasmonics for future biosensors. Nat Photonic **6**, 709–613 (2012)

Bag, S.K., Wan, M., Sinha, R.K., Varshney, S.K.: Design and characterization of surface relief grating on etched multimode optical fiber for refractive index sensing. Sens. Actuators A **303**, 111836 (2020)

Chang, J.F., Kuo, H.H., Leu, I.C., Hon, M.H.: The effects of thickness and operation temperature on ZnO: Al thin film CO gas sensor. Sens. Actuators B Chem. **84**(2–3), 258–264 (2002)

Chen, X., Xia, L., Li, C.: Surface plasmon resonance sensor based on a novel D-shaped photonic crystal fiber for low refractive index detection. IEEE Photonics J. **10**(1), 6800709 (2018)

Chi, C., Chen, H., Chen, W., Chang, C., Liu, W.: Formaldehyde sensing characteristics of an aluminum-doped zinc oxide (AZO) thin-film-based sensor. Sens. Actuators B Chem. **255**, 3017–3024 (2018)

Dean, A.J.: Lange'S Chemistry Handbook. McGraw-Hill Book Company, New York (1998)

Gupta, B.D., Verma, R.: Surface plasmon resonance based optical fiber sensors: principle, probe designs and some applications. J Sens. **2009**, 979761 (2009)

Haque, E., Hossain, M.A., Namihira, Y., Ahmed, F.: Microchannel-based plasmonic refractive index sensor for low refractive index detection. Appl. Opt. **58**, 1547–1554 (2019a)

Haque, E., Mahmuda, S., Hossain, M.A., Hai, N.H., Namihira, Y., Ahmed, F.: Highly sensitive dual-core PCF based plasmonic refractive index sensor for low refractive index detection. IEEE Photonics J. **11**(5), 7905309 (2019b)

Harith, Z., Batumalay, M., Irawati, N., Harun, S., Arof, W.H., Ahmad, H.: Relative humidity sensor employing tapered plastic optical fiber coated with seeded Al-doped ZnO. Optik **144**, 257–262 (2017)

Harith, Z., Irawati, N., Rafaie, H.A., Batumalay, M., Harun, S.W., Nor, R.M., Ahmad, H.: Tapered plastic optical fiber coated with Al-doped ZnO nanostructures for detecting relative humidity. IEEE Sens. J. **15**(2), 845–849 (2015)

Harris, R.D., Wilkinson, J.S.: Waveguide surface plasmon resonance sensors. Sens. Actuator B **29**(95), 261–267 (1995)

Hassani, A., Skorobogatiy, M.: Photonic crystal fiber based plasmonic sensors for the detection of biolayer thickness. J. Opt. Soc. Am. B **26**(8), 1550–1557 (2009)

Homola, J.: Surface plasmon resonance sensors for detection of chemical and biological species. Chem. Rev. **108**, 462–493 (2008)

Islam, M.R., Khan, M.M.I., Mehjabin, F., Chowdhury, J.A., Islam, M.: Design of a fabrication friendly & highly sensitive surface plasmon resonance-based photonic crystal fiber biosensor. Results Phys. **19**, 103501 (2020)

Islam, M.R., Khan, M.M.I., Siraz, S., Mehjabin, F., Rahman, M., Islam, M., Anzum, M.S., Chowdhury, J.A., Noor, F.: Design and analysis of a QC-SPR-PCF sensor for multipurpose sensing with supremely high FOM. Appl. Nanosci. **12**(1), 29–45 (2022)

Jain, S., Choudhary, K., Kumar, S.: Photonic crystal fiber-based SPR sensor for broad range of refractive index sensing applications. Opt. Fiber Technol. **73(1)**, 103030 (2022)

Kanmania, R., Zainuddinb, N.A.M., Rusdic, M.F.M., Harunc, S.W., Ahmedd, K., Amirif, I.S., Zakariab, R.: Effects of TiO2 on the performance of silver coated on side-polished optical fiber for alcohol sensing applications. Opt. Fiber Technol. **50**, 183–187 (2019)

Karki, B., Jha, A., Pal, A., Srivastava, V.: Sensitivity enhancement of refractive index-based surface plasmon resonance sensor for glucose detection. Opt. Quant. Electron. **54**, 595 (2022a)

Karki, B., Ramya, K.C., Sandhya Devi, R.S., Srivastava, V., Pal, A.: Titanium dioxide, black phosphorus and bimetallic layer-based surface plasmon biosensor for formalin detection: numerical analysis. Opt. Quantum Electron. **54**, 451 (2022b)

Karki, B., Uniyal, A., Pal, A., Srivastava, V.: Advances in surface plasmon resonance-based biosensor technologies for cancer cell detection. Int. J. Opt. **2022**, 1–10 (2022c)

Karki, B., Vasudevan, B., Uniyal, A., Pal, A., Srivastava, V.: Hemoglobin detection in blood samples using a graphene-based surface plasmon resonance biosensor. Optik **270**, 169947 (2022d)

Karki, B., Trabelsi, Y., Uniyal, A., Pal, A.: Zinc sulfide, silicon dioxide, and black phosphorus based ultra-sensitive surface plasmon biosensor. Opt. Quant. Electron. **54**, 107 (2022e)

Karki, B., Uniyal, A., Srivastava, G., Pal, A.: Black phosphorous and cytop nanofilm-based long-range SPR sensor with enhanced quality factor. J. Sens. **2023**, 1–10 (2023)

Kaur, B., Kumar, S., Kaushik, B.K.: MXenes-based fiber-optic SPR sensor for colorectal cancer diagnosis. IEEE Sens. J. **22**(7), 6661–6668 (2022)

Kretschmann, E., Raether, H.: Radiative decay of non-radiative surface plasmons ecxited by the light. Natureforsch. A **23**, 2135–2136 (1968)

Kumar, H., Ramani, U., Singh, B.K., Pandey, P.C.: Investigations on the highly sensitive metal-coated broad range D-shaped optical fiber refractive index sensor. Plasmonics **16**(6), 1963–1971 (2021)

Lee, B., Roh, S., Park, J.: Current status of micro- and nano-structured optical fiber sensors. Opt. Fiber Technol. **15**(3), 3–15 (1999)

Li, L., Zhang, X., Liang, Y., Guang, J., Peng, W.: Dual-channel fiber surface plasmon resonance biological sensor based on a hybrid interrogation of intensity and wavelength modulation. J Biomed. Opt. **21(12)**, 127001 (2016)

Liu, B.H., Jiang, Y.X., Zhu, X.S., Tang, X.L., Shi, Y.W.: Hollow fiber surface plasmon resonance sensor for the detection of liquid with high refractive index. Opt. Express **21**(26), 32349–32357 (2013)

Liu, C., Yang, L., Liu, Q., Wang, F., Sun, Z., Sun, T., Mu, H., Chu, P.K.: Analysis of a surface plasmon resonance probe based on photonic crystal fibers for low refractive index detection. Plasmonics **13**, 779–784 (2018)

Liu, C., Wang, J., Wang, F., Su, W., Yang, L., Lv, J., Fu, G., Li, X., Liu, Q., Sun, T., Chu, P.K.: Surface plasmon resonance (SPR) infrared sensor based on D-shape photonic crystal fibers with ITO coatings. Opt. Commun. **464**, 125496 (2020)

Ma, Y., Du, G.T., Yang, S.R., Li, Z.T., Zhao, B.J., Yang, X.T., Yang, T.P., Zhang, Y.T., Liu, D.L.: Control of conductivity type in undoped ZnO thin films grown by metalorganic vapor phase epitaxy. J. Appl. Phys. **95**(11), 6268–6272 (2004)

Mishra, S.K., Mishra, A.K.: ITO/Polymer matrix assisted surface plasmon resonance based fiber optic sensor. Results Opt. **5**, 100173 (2021)

Mridha, S., Basak, D.: Aluminium doped ZnO film: electric, optical and photoresponse studies. J. Phys. d: Appl. Phys. **40**(22), 746–750 (2007)

Nayak, J.K., Jha, R.: Numerical simulation on the performance analysis of a graphene-coated optical fiber plasmonic sensor at anti-crossing. Appl. Opt. **56**(12), 3510–3517 (2017)

Prieto-Cortés, P., Álvarez-Tamayo, R.I., García-Méndez, M., Durán-Sánchez, M.: Lossy mode resonance generation on sputtered aluminum-doped zinc oxide thin films deposited on multimode optical fiber structures for sensing applications in the 1.55 μm wavelength range. Sensors **19**, 4189 (2019)

Paliwal, N., John, J.: Theoretical modeling and investigations of AZO coated LMR based fiber optic tapered tip sensor utilizing an additional TiO^2 layer for sensitivity enhancement. Sens. Actuators B Chem. **238**, 1–8 (2017)

Paul, A.K., Sarkar, A.K., Razzak, S.M.A.: Graphene coated photonic crystal fiber biosensor based on surface plasmon resonance. 2017 IEEE Region 10 Humanitarian Technology Conference (R10-HTC), 856–859 (2017)

Paul, A.K., Sarkar, A.K., Khaleque, A.: Dual-core photonic crystal fiber plasmonic refractive index sensor: a numerical analysis. Photon. Sens. **9**, 151–161 (2019)

Raether, H.: Surface Plasmons on Smooth and Rough Surfaces and on Gratings, vol. 111, pp. 1–133. Springer, Berlin (1988)

Rhodes, C., Franzen, S.: Surface plasmon resonance in conducting metal oxides. J. Appl. Phys. **100**, 054905 (2006)

Saeed, A.H.E., Khalil, A.E., Hameed, M.F.O., Azab, M.Y., Obayya, S.S.A.: Highly sensitive SPR PCF biosensors based on Ag/TiN and Ag/ZrN configurations. Opt. Quantum Electron. **51**, 56 (2019)

Sazio, P.J., Amezcua-Correa, A., Finlayson, C.E., Hayes, J.R., Scheidemantel, T.J., Baril, N.F., Jackson, B.R., Won, D.J., Zhang, F., Margine, E.R., Gopalan, V.: Microstructured optical fibers as high-pressure microfluidic reactors. Science **311**(5767), 1583–1586 (2006)

Sharma, A.K., Gupta, B.D.: On the performance of different bimetallic combination in surface plasmon resonance based fiber optic sensor. J. Appl. Phys. **101**, 093111 (2007)

Shi, Y.W., Ito, K., Ma, L., Yoshida, T., Matsuura, Y., Miyagi, M.: Fabrication of a polymer-coated silver hollow optical fiber with high performance. Appl. Opt. **45**(26), 6736–6740 (2006)

Shukla, S., Sharma, N.K., Sajal, V.: Sensitivity enhancement of a surface plasmon resonance based fiber optic sensor using ZnO thin film: a theoretical study. Sens. Actuators B **206**, 463–470 (2015)

Singh, P.K., Singh, V.K., Chualya, S.K.: Numerical analysis of LSPR based fiber sensor for low refractive index detection. Optik **224**, 165704 (2020)

Tan, C.Z.: Determination of refractive index of silica glass for infrared wavelength by IR spectroscopy. J. Non-Cryst. Solids **223**, 158–163 (1998)

Tsai, W., Lin, K., Yang, S., Tsao, Y., Ho, P.J.: Fiber-optic surface plasmon resonance-based sensor with AZO/Au bilayered sensing layer. Chin. Opt. Lett. **12**(4), 042801 (2014)

Wang, F.M., Liu, C., Sun, Z.J., Sun, T., Liu, B.H., Chu, P.K.: A highly sensitive SPR sensors based on two parallel PCFs for low refractive index detection. IEEE Photon. J. **10(4)**, 7104010 (2018)

Wang, T., Zhang, M., Liu, K., Jiang, J., Zhao, Y., Ma, J., Liu, T.: The effect of the TiO_2 film on the performance of the fiber optic SPR sensor. Opt Commun. **448**, 93–97 (2019)

Xing, L., Zheng, Y., Sun, Y., Wang, M., Cui, H., Li, T.: Optical fiber sensor determination of the water salinity based on surface plasmon resonance. Infrared Laser Eng. **44**(4), 1290–1296 (2015)
Yadav, M.K., Kumar, P., Verma, R.K.: Detection of adulteration in pure honey utilizing Ag-graphene oxide coated fiber optic SPR probes. Food Chem. **332**, 127346 (2020)
Yang, Z., Xia, L., Li, C., Chen, X., Liu, D.: A surface plamon resonance sensor based on concave-shaped photonic crystal fiber for low refractive detection. Opt. Commun. **430**, 195–203 (2019)
Zhang, S., Guo, Y., Cheng, T., Li, S., Li, J.: Surface plasmon resonance sensor based on a D-shaped photonic crystal fiber for high and low refractive index detection. Optik **212**, 164697 (2020)
Zhao, Y., Deng, Z., Li, J.: Photonic crystal fiber based surface plasmon resonance chemical sensors. Sens. Actuators B Chem. **202**, 557–567 (2014)